Mechanized deep tunnel excavation in saturated clayey soils

A pre-design hydro-mechanically coupled method for the assessment of both spoil and face volume loss

Flessati, Luca; Di Prisco, Claudio

DOI
10.1680/jgeot.23.00294

Publication date
2024

Document Version
Final published version

Published in
Geotechnique

Flessati, L. & Di Prisco, C. *Géotechnique* [https://doi.org/10.1680/jgeot.23.00294]

Mechanised deep tunnel excavation in saturated clayey soils: a pre-design hydro-mechanically coupled method for the assessment of both spoil and face volume loss

LUCA FLESSATI* and CLAUDIO DI PRISCO†

Mechanised tunnel excavation in soils causes over-excavations, potentially leading to large amounts of spoil and settlements at ground level. An accurate estimation of over-excavations is crucial in the pre-design phase for assessing costs, determining the appropriate excavation method and choosing the muck management strategy. Currently, the estimation is based on experience and data from similar projects, but this becomes difficult when project conditions are heterogeneous. As an alternative, finite-element analyses are time-consuming and not suitable for early design stages; therefore, simplified tools are needed. In this paper, the authors present a simplified approach putting in relation face extrusion with estimated spoil mass and face volume loss. This approach, conceived for deep tunnels, is the extension to the case of mechanised tunnelling of a hydro-mechanical coupled meta-model derived from finite-element numerical analyses for tunnels in clayey soils excavated by using conventional techniques (i.e. without any use of tunnel-boring machines). The model has been validated against field data relative to a case study. The approach can be used in the early design process to identify tunnel-boring machine characteristics and provide preliminary cost estimates. In addition, during the construction phase, the method can be employed to interpret monitoring data and pre-design mitigation measures for unforeseen soil profile variations.

KEYWORDS: excavation; face characteristic curve; face extrusion; meta-model; spoil; tunnels & tunnelling; volume loss

INTRODUCTION

Excavating tunnels in soils may cause over-excavations, potentially resulting in large spoil masses and unexpected settlements at the ground level. An accurate estimation of the extent of over-excavation is crucial during the early design stages, such as planning and feasibility studies, as it allows: (*a*) the estimation of excavation costs and (*b*) the selection of the most suitable excavation method and muck management strategy. Currently, the estimation of over-excavation is frequently based on experience and data gathered from similar projects, using the volume loss (the non-dimensional ratio of the volume per unit tunnel length of settlement trough at a given depth (usually at or near the surface) and the area of the excavated tunnel) as an indirect measure. However, when significant variations in project conditions are expected, the prediction of volume loss becomes very challenging without performing time-consuming non-linear finite-element (FE) numerical analyses. Obviously, these analyses are not compatible with early design stages, where uncertainties regarding the mechanical behaviour of materials are unavoidable, and multiple potential solutions and mitigation strategies need to be considered. During early design phases, when preliminary cost has to be estimated and the most suitable excavation method is chosen, simplified tools must be employed.

As is suggested by many authors (Attewell & Farmer, 1974; Cording & Hansmire, 1975; Mair & Taylor, 1997; Vu *et al.*, 2016), volume losses associated with mechanised tunnelling are usually calculated by adding four components: (*a*) volume loss at the tunnel face; (*b*) volume loss along the shield; (*c*) volume loss at the tail; and (*d*) long-term volume loss due to consolidation. Among these four contributions, only the first one is related to the spoil mass. This is also associated with the face extrusion (i.e. the movement of soil toward the excavation chamber induced by the variation in stresses in the advance core), therefore, its estimation requires the analysis of the mechanical response of the face. In the past, numerous authors have addressed this topic from various perspectives, including theoretical, experimental, and numerical analyses.

In the literature, theoretical studies are mainly based on either the limit equilibrium method (Horn, 1961; Anagnostou & Kovari, 1996) or the limit analysis theory (Davis *et al.*, 1980; Mühlhaus, 1985; Leca & Dormieux, 1990; Wong & Subrin, 2006; Klar *et al.*, 2007; Mollon *et al.*, 2009, 2013; Pferdekämper & Anagnostou, 2022). Both the approaches allow the assessment of the minimum pressure to prevent face collapse, but not face extrusion.

From an experimental point of view, both centrifuge (Mair, 1979; Kimura & Mair, 1981; Chambon & Corté, 1994; Nomoto *et al.*, 1999; Kamata & Mashimo, 2003) and $1g$ small-scale model tests (Sterpi & Cividini, 2004; Kirsch, 2009; Berthoz *et al.*, 2012a, 2012b; Chen *et al.*, 2013; Hu *et al.*, 2022; Shang *et al*, 2023) were performed to study the minimum pressure to be applied on the face to ensure its stability. Therefore, these studies cannot be directly used to provide an estimation of face extrusion. As far as $1g$ small-scale model tests are concerned, particularly

Manuscript received 11 September 2023; revised manuscript accepted 12 March 2024. First published online ahead of print 25 March 2024.
Discussion on this paper is welcomed by the editor.
* Faculty of Civil Engineering and Geoscience, Delft University of Technology, Delft, the Netherlands.
† Department of Civil and Environmental Engineering, Politecnico di Milano, Milan, Italy.

interesting are the results in di Prisco *et al.* (2018a), in which the influence of the hydro-mechanical (HM) coupling on the face response is discussed. The experimental results clearly put in evidence the fundamental role of the excavation rate on face extrusion and, on the basis of the experimental results, a simplified approach to estimate the minimum excavation rate, under which the face mechanical response become unstable, was proposed.

The importance of the role of HM coupling in affecting the face response has also been numerically put in evidence by many authors by performing FE numerical analyses (Callari, 2004, 2015; Callari & Casini, 2006; Höfle *et al.*, 2008, 2009; Sitarenios & Kavvadas, 2016; Callari *et al.*, 2017; Soe & Ukritchon, 2023).

Finite-element numerical results have also recently been used to introduce 'meta-models' (i.e. 'upscaled models' or 'surrogate models') suitable for deep tunnels excavated by means of conventional tunnelling in saturated clayey soils (di Prisco *et al.*, 2018b, 2019a, 2019b, 2020; Flessati & di Prisco, 2022, 2023). These meta-models are capable of replicating FE results in relation to face extrusion and, once tunnel geometry and soil properties are assigned, they can be employed to preliminarily calculate face extrusion without the need for conducting FE simulations.

The objectives of this paper are:

(*a*) to extend the meta-model introduced in di Prisco *et al.* (2019b) to the case of mechanised tunnelling
(*b*) to present a new simplified method putting in relation face extrusion and advancement rate for a tunnel excavated in saturated soils
(*c*) to estimate both spoil mass and volume loss at the tunnel face accounting for HM coupling
(*d*) validate the method by comparing its blind predictions with field data.

This new method is a valuable tool to be used in the early design stages to provide a preliminary estimate of both the costs associated with the spoil management and the surface settlements. It is worth mentioning that this simplified approach is not intended to be used during the detailed and for-construction design, when advanced FE simulations, reproducing in detail the tunnel-boring machine (TBM) subsystems, are required. An exhaustive and recent discussion of this topic is reported in Kratz *et al.* (2023).

For the sake of clarity, in the section titled 'Meta-model for the assessment of HM coupled face extrusion' the meta-model introduced in di Prisco *et al.* (2019b) is briefly summarised. In the section 'Application to the case of mechanised tunnelling', its extension to mechanised tunnelling is presented, and finally, in the section 'Application to a case study', its practical application to a case study is illustrated.

META-MODEL FOR THE ASSESSMENT OF HM COUPLED FACE EXTRUSION

The meta-model introduced in di Prisco *et al.* (2019b) is a relationship (named characteristic curve) between average face pressure (σ_f), excavation rate (v_{ex}) and average face extrusion (u_f). This does not imply that the stresses on the face and face displacement distributions are uniform. To conceive this meta-model and to train it, the results of a series of non-linear three-dimensional (3D) FE numerical analyses were used.

The assumptions of both HM coupled numerical analyses and meta-model are listed below.

(*a*) The tunnel cross-section is circular and the diameter is termed D.
(*b*) The cover diameter ratio (H/D) is assumed to be sufficiently large ($H/D > 4$) to neglect the effect of the ground surface ('deep tunnel').
(*c*) The water table is at the ground surface.
(*d*) The tunnel is excavated in a saturated homogeneous soil layer characterised by a unit weight (γ_{sat}) constant along depth.
(*e*) The hydraulic behaviour is isotropic and permeability (k) is constant along the depth.
(*f*) The lining is rigid and impervious to water.
(*g*) The excavation process is modelled as a progressive reduction in the pressure applied on the tunnel face and the time t_u to complete the face unloading is assumed to be coincident with the time necessary to excavate a tunnel length $L_a = 1{\cdot}5D$ (L_a is the distance from the face at which stresses are practically not affected by the excavation, as is shown in di Prisco *et al.*, 2022a), implying that $v_{ex} = 1{\cdot}5D/t_u$.
(*h*) The soil behaviour is reproduced by using an elastic–perfectly plastic constitutive relationship with a Mohr–Coulomb failure criterion and a non-associated flow rule (nil dilatancy). In fact, when an elastic–perfectly plastic constitutive relationship is employed to simulate the mechanical behaviour of a clay, the dilatancy at failure (i.e. at critical state) has to be nil.

Additional details regarding the numerical model are reported in Appendix 1.

For the sake of generality, the meta-model is defined by using the following non-dimensional variables:

$$Q_f = \frac{\sigma_{f0} - \sigma_f}{S_u^*} \quad q_f = \frac{u_f}{u_{f,relu}} \frac{\sigma_{f0}}{S_u^*} \quad \Upsilon = \frac{3(1-2\nu)\gamma_w D^2}{kEt_u} \tag{1}$$

where σ_{f0} is the initial (geostatic) value of σ_f; γ_w is the water unit weight; ν is the Poisson's ratio; and E is the Young's modulus of the soil, assumed to be constant in the soil domain. S_u^* is a strength parameter depending on the boundary value problem accounted for and can be written as: $S_u^* = \alpha S_{u,e}$. α only depends on friction angle ϕ' (Appendix 2). $S_{u,e}$ is the value of the soil's undrained strength calculated (by adopting the constitutive relationship used for the FE simulations) by imposing the geostatic effective pressure at tunnel axis depth (p^*) and an undrained extension stress path ($S_{(u,e)}/p^* = M_e/2$, where $M_e = 6\sin\phi'/(3+\sin\phi')$). $u_{f,relu}$ represents the undrained elastic residual (i.e. for $\sigma_f = 0$) face extrusion (di Prisco *et al.*, 2018b):

$$u_{f,relu} = \frac{2}{3}\frac{1+\nu}{K_{el}}\frac{\sigma_{f0}}{E}D \tag{2}$$

where K_{el} is a non-dimensional parameter depending on the H/D value. The numerical FE results reported in di Prisco *et al.* (2018b) make it possible to conclude that, for $H/D > 5$, K_{el} is practically constant and equal to 3.

The non-dimensional definitions of variables Q_f and q_f come from the analytical solution of undrained tunnel cavities in unbounded media (di Prisco *et al.*, 2018b), whereas the non-dimensional definition of Υ comes from the equation of mass balance of water (Appendix 3). The definition of the meta-model in terms of non-dimensional variables makes the meta-model reliable for any geometry/soil property value, extending infinitely its range of applicability.

According to di Prisco *et al.* (2019b), the use of these non-dimensional variables is particularly convenient since, for any given value of Υ, a unique global (characteristic curve) and local (stress, pore pressure, strains and displacement fields) response, independent of both geometry and soil hydraulic/mechanical properties, is obtained (Appendix 4).

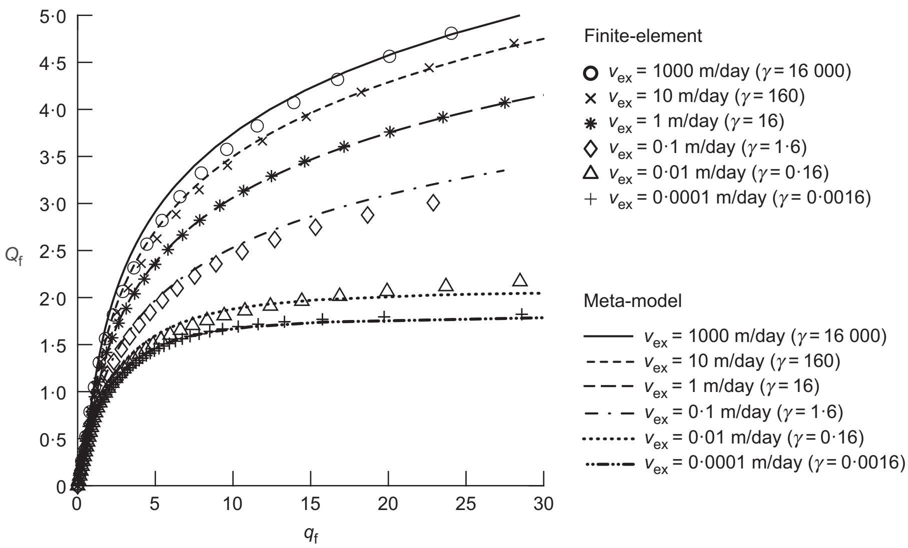

Fig. 1. Non-dimensional face characteristic curves

Table 1. Geometry and soil mechanical/hydraulic properties

D: m	H/D	E: MPa	ν	c': kPa	ϕ': deg	ψ: deg	γ_{sat}: kN/m^3	k: m/s
15	7	85	0·3	0	25	0	20	10^{-9}

According to the meta-model, the relation between Q_f and q_f can be expressed as follows:

$$q_f(Q_f, \Upsilon) = \begin{cases} \dfrac{Q_f}{R(\Upsilon)}, & Q_f < a_f(\Upsilon) \\ \dfrac{a_f(\Upsilon)}{R(\Upsilon)} e^{Q_f/a_f(\Upsilon)} + \dfrac{Q_f - a_f(\Upsilon)}{Q_L(\Upsilon) - Q_f}, & Q_f > a_f(\Upsilon) \end{cases} \quad (3)$$

where $R(\Upsilon)$, $a_f(\Upsilon)$ and $Q_L(\Upsilon)$ are functions governing, respectively, the initial inclination of the characteristic curves, the transition from the initial linear to non-linear response and the limit/collapse value for Q_f. The training of the model consisted in using FE results to define the functions $R(\Upsilon)$, $a_f(\Upsilon)$ and $Q_L(\Upsilon)$ (Appendix 5).

The characteristic curves obtained by using this meta-model (solid and dashed lines) are compared in Fig. 1 with FE numerical results (symbols). Geometry and soil properties employed to obtain the numerical results are reported in Table 1. In these cases, the at-rest lateral earth pressure (k_0) is assumed to be equal to one and different values of v_{ex} were considered. An extension to different k_0 values is quite simple and implies only a change in one meta-model parameter (a_{fu} defined in Appendix 5). As is evident in Fig. 1 the meta-model can satisfactorily reproduce FE results for any value.

Despite the simplicity of the constitutive relationship adopted, the numerical results capture very satisfactorily the mechanical processes taking place in the soil domain. Testament to this is the slight dependence of non-dimensional face characteristic curves on the constitutive relationship implemented in the numerical code. In Flessati & di Prisco (2018) the authors illustrated the non-dimensional characteristic curves obtained by implementing the modified Cam Clay model and showed that the correct assessment of S_u^* allows curves to be obtained that are practically coincident with those obtained by using an elastic–perfectly plastic constitutive relationship.

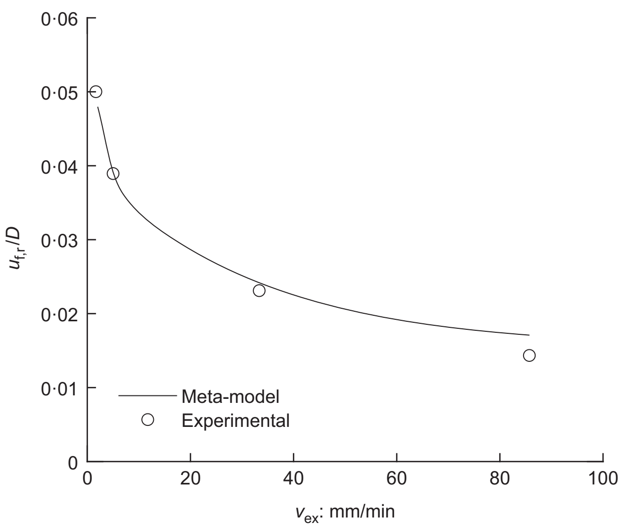

Fig. 2. Comparison between blind predictions with the meta-model and experimental results (adapted from di Prisco *et al.* (2018a))

In di Prisco *et al.* (2019b) the meta-model is also validated by using the results of a series of 1***g*** small-scale model experimental tests (tests A1–A4 of di Prisco *et al.* (2018a)). The hydro/mechanical properties of the soil employed correspond to those of the material employed for the small-scale tests (Flessati, 2017). In Fig. 2, the residual displacements ($u_{f,r}$) are illustrated plotted against v_{ex}. Again, the agreement is satisfactory.

An alternative representation of equation (3) is provided in Fig. 3(a), where iso-q_f curves are plotted. All these curves are characterised by two horizontal branches, one for small ($\Upsilon < 10^{-1}$) and one for large ($\Upsilon > 10^4$) Υ values, corresponding, respectively, to drained and undrained face responses. All the other Υ values ($10^{-1} < \Upsilon < 10^4$) identify 'partially drained' face responses. In this Υ range, the face response

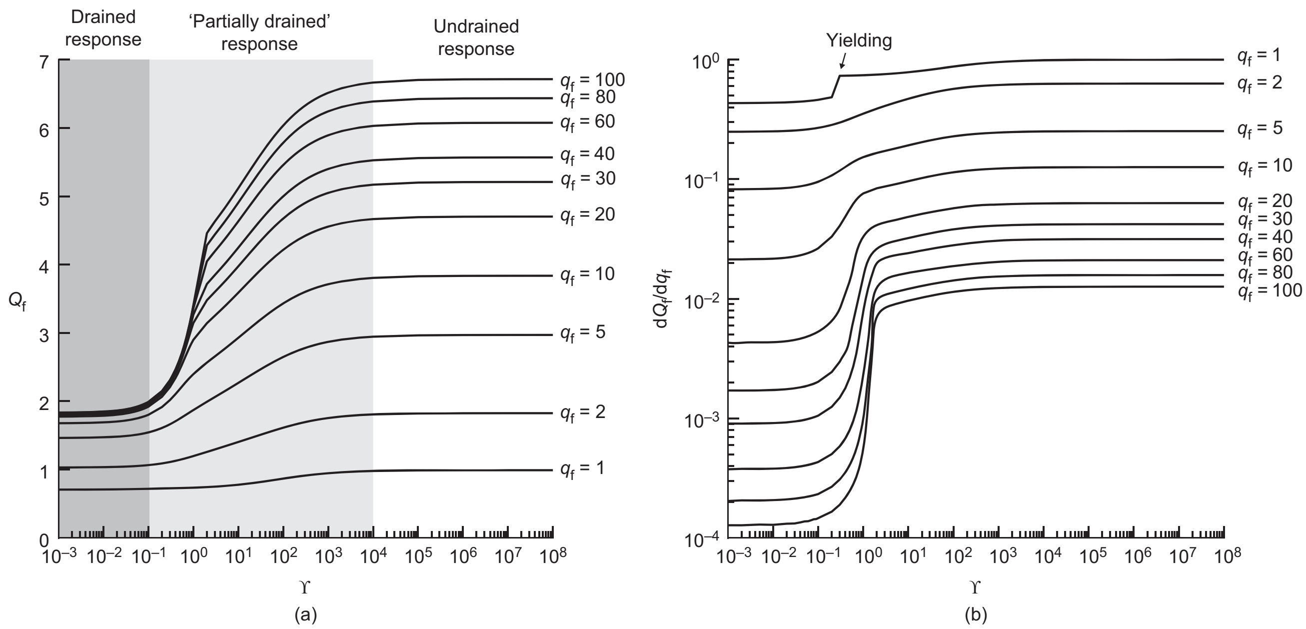

Fig. 3. Tunnel face characteristic curves: (a) in the Q_f–ϒ plane and (b) in the dQ_f/dq_f–ϒ plane

is significantly affected by ϒ (in particular in the interval $1 < ϒ < 10$), implying that increases/reductions in the excavation rate may significantly decrease/increase face extrusion. Fig. 3(a) is a very useful tool in the early phases of the pre-design stage, since it allows, with a negligible computational effort (only the definition of both geometry/soil properties and the calculation of the non-dimensional variables are required), estimation of the face displacements associated with an assigned excavation rate.

It is worth mentioning that, in the case of deep tunnels, for large excavation rates (undrained response), the system is not characterised by the development of a failure mechanism (as is observed in di Prisco *et al.* (2018b), the stiffness of the characteristic curve never nullifies), although the extrusion values may be unacceptable. In other words, from a mechanical point of view, the knowledge of a face extrusion value (or equivalently of volume loss at the tunnel face) does not provide a priori hints on the stability of the face. To clarify this concept, in Fig. 3(b) the variation in the characteristic curve stiffness (dQ_f/dq_f) with ϒ is plotted. Each curve corresponds to a different q_f value. As is expected, for all the q_f values, a decrease in ϒ is associated with a reduction in stiffness. For large q_f values ($q_f > 20$), a very pronounced reduction in stiffness is evident for $ϒ < 5$. This implies that for $ϒ < 5$ the face may be at failure.

APPLICATION TO THE CASE OF MECHANISED TUNNELLING

As was previously mentioned, the meta-model briefly outlined in the previous section was originally conceived for conventional tunnelling, that is for unsupported faces for which extrusion ($q_f = q_{fus}$, where 'us' stands for unsupported, Fig. 4) is calculated by imposing in equation (3) $\sigma_f = 0$ and

$$Q_f = Q_{fus} = \frac{\sigma_{f0}}{S_u^*} \tag{4}$$

In contrast, in case of mechanised tunnelling, face extrusion ($q_f = q_{fs}$, where 's' stands for supported, Fig. 4) has to be calculated by imposing:

$$Q_f = Q_{fs} = \frac{\sigma_{f0} - \sigma_{f,TBM}}{S_u^*} = Q_{fus} - Q_{TBM} \tag{5}$$

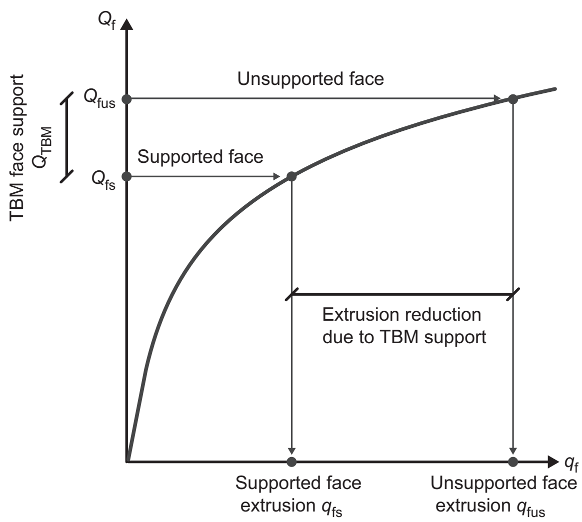

Fig. 4. Face extrusion reduction due to TBM face pressure

where $\sigma_{f,TBM}$ is the pressure applied on the tunnel face by the TBM head. As is expected, the larger the TBM face pressure, the smaller is the face extrusion (Fig. 4).

As was previously mentioned, from a design standpoint, the meta-model offers the advantage of providing an initial assessment of face extrusion without the need to perform any FE numerical simulations. In the subsequent sections, the extrusion value will be used, by following a novel procedure, to estimate spoil mass and volume loss at the tunnel face, accounting for the HM coupling. Moreover, apart from this direct application, the meta-model can also be employed in the preliminary design phase for two additional purposes: (*a*) determining whether face support is necessary and (*b*) selecting $\sigma_{f,TBM}$ based on a displacement-based design approach (Fig. 5).

In this case the meta-model is used as it follows.

(*a*) ϒ and Q_{fus} are calculated by means of equations (1) and (4), respectively.
(*b*) The value of the unsupported face extrusion (q_{fus}) is calculated by introducing ϒ and Q_{fus} in equation (3).

(*c*) A value of admissible face extrusion $u_{f,adm}$ is assigned (e.g. from limitations on the maximum admissible volume loss) and by using equation (1) the corresponding non-dimensional value ($q_{f,adm}$) is calculated.

(*d*) If $q_{fus} < q_{f,adm}$, face support is not required, whereas if $q_{fus} > Q_{f,adm}$, face support is required. In this second case, Q_{fs} is calculated by imposing $q_f = q_{f,adm}$, in equation (3) and finally and $\sigma_{f,TBM}$ is calculated by using equation (5).

Even during the excavation, the meta-model is very useful since it allows (*a*) alongside monitoring data, to confirm the design assumptions related to soil hydraulic and mechanical properties and (*b*) to choose potential counter-measures such as either adjusting face pressure or advance rate in response to unforeseen and inevitable soil profile changes.

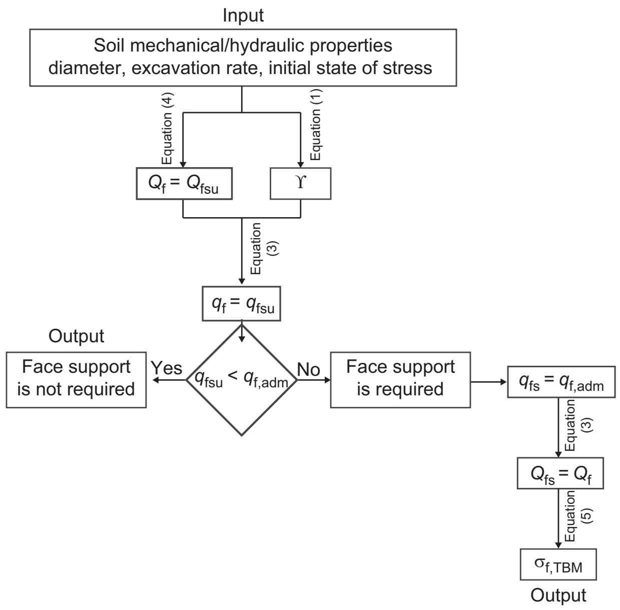

Fig. 5. Design of TBM face pressure

Spoil weight assessment

As a first approximation, the spoil weight extracted for each segmental lining ring (W_s) can be calculated by summing a term W_r, related to the volume of the ideal excavation cross-section of length L_r (the lining segment length) and a term W_e varying with advance rate and face pressure, related to u_f:

$$W_s = W_r + W_e = \frac{\gamma_{sat}\pi D^2}{4} L_r + \frac{\gamma_{sat}\pi D^2}{4} u_f \tag{6}$$

The dependence of W_s on both $\sigma_{f,TBM}$ and v_{ex} is illustrated in Fig. 6, for $L_r = 2$ m and for the geometry and soil properties of Table 1. The four lines represented in Fig. 6(a) are obtained by imposing $v_{ex} = 1$, 2, 5 and 10 m/day, whereas the two lines of Fig. 6(b) are obtained by imposing $\sigma_{f,TBM} = 180$ and 360 kPa.

As was expected, for a fixed value of v_{ex}, a reduction in $\sigma_{f,TBM}$ implies an increase in W_s (Fig. 6(a)). The minimum W_s value ($W_s = W_r$) corresponds to the (ideal) case $\sigma_{f,TBM} = \sigma_{f0}$, for which over-excavation is nil ($u_f = 0$).

The results of Fig. 6(b) highlight that, as was expected, W_s decreases by increasing the excavation rate. Nevertheless, for the case considered ($D = 15$ m, $k = 10^{-9}$ m/s and $E = 85$ MPa) this reduction is practically negligible for $v_{ex} > 10$ m/day, since for $v_{ex} > 10$ m/day the system response is practically undrained. However, this result is not general and is strictly dependent on both soil permeability and tunnel diameter (equation (3)).

At face volume loss assessment

Under the assumption that the tunnel face effect propagates for a length L_a (di Prisco *et al.*, 2022a), it is possible to write that

$$V_{L,f} = \frac{u_f}{L_a} \tag{7}$$

where $V_{L,f}$ is the volume loss at the face.

In Fig. 7 the dependence of $V_{L,f}$ with both $\sigma_{f,TBM}$ and v_{ex} is illustrated for the reference case (Table 1). The four curves of Fig. 7(a) refer to $v_{ex} = 1$, 2, 5 and 10 m/day, whereas the

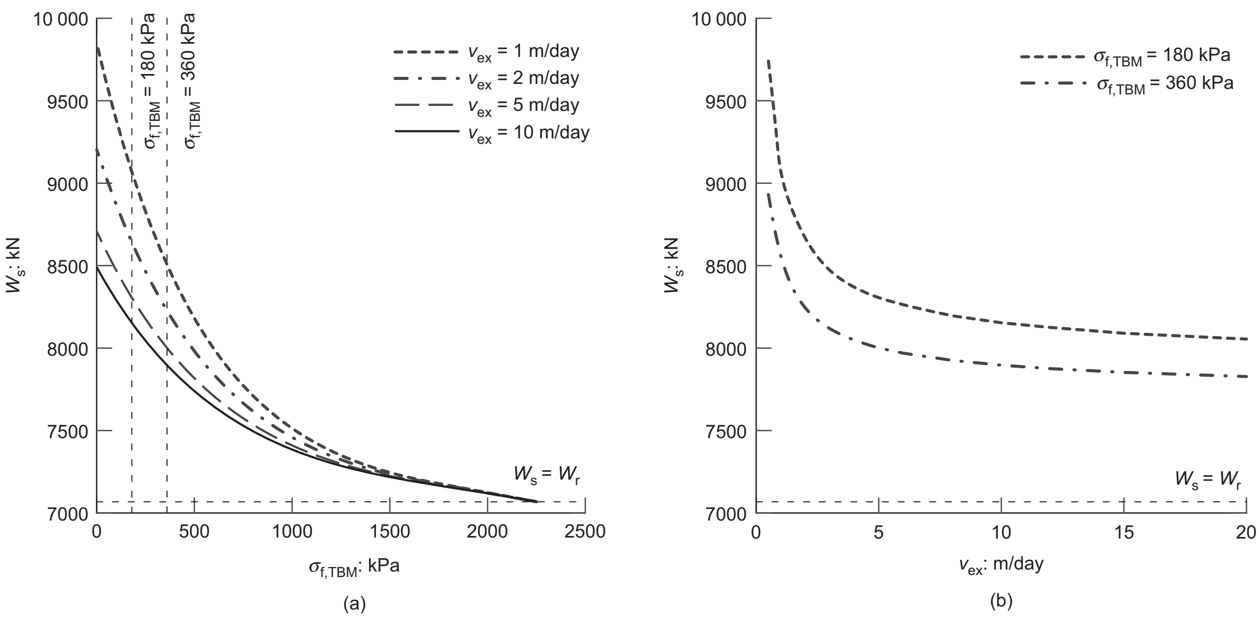

Fig. 6. Variation of W_s with (a) TBM face pressure (v_{ex} = 1–10 m/day) and (b) excavation rate ($\sigma_{f,TBM}$ = 180, 360 kPa)

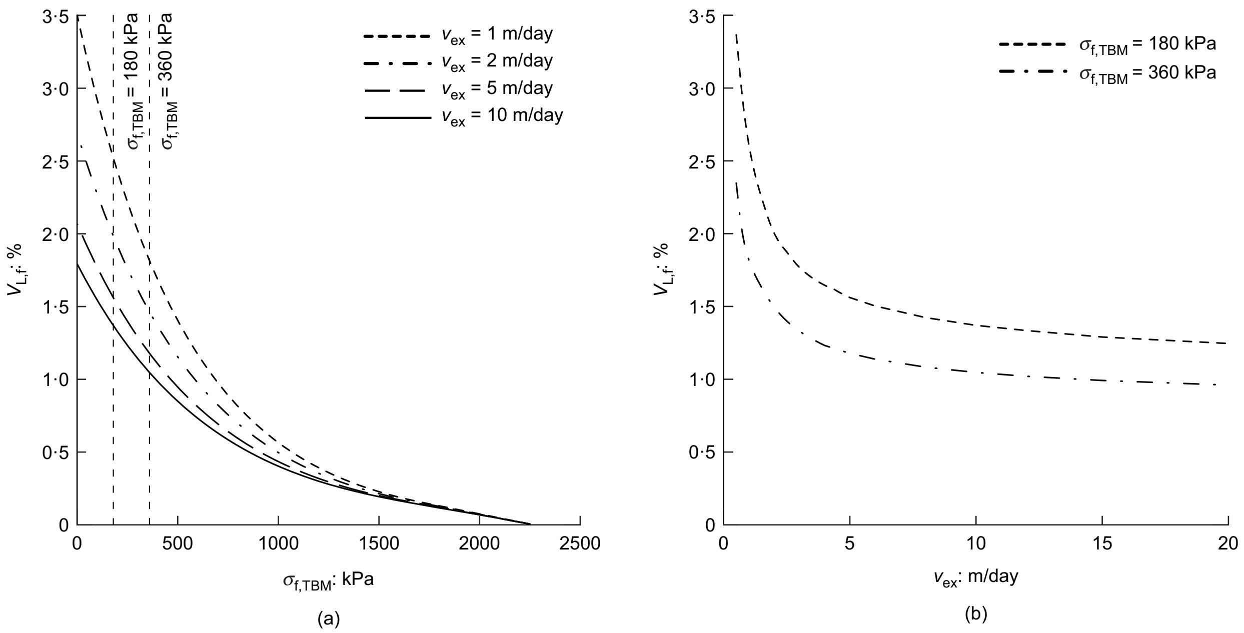

Fig. 7. Variation of $V_{L,f}$ with (a) TBM face pressure (v_{ex} = 1–10 m/day) and (b) excavation rate ($\sigma_{f,TBM}$ = 180, 360 kPa)

results in Fig. 7(b) refer to two values of $\sigma_{f,TBM}$ (180 and 360 kPa).

As was expected, a reduction in $\sigma_{f,TBM}$ implies an increase in $V_{L,f}$ (Fig. 7(a)) and the minimum value of zero corresponds to the ideal case $\sigma_{f,TBM} = \sigma_{f0}$, for which $u_f = 0$.

$V_{L,f}$ decreases by increasing the excavation rate. Nevertheless, for the case considered (D = 15 m, $k = 10^{-9}$ m/s and E = 85 MPa) this reduction is practically negligible for $v_{ex} > 10$ m/day, but this result is not general since it depends on soil permeability and tunnel diameter (equation (3)).

It is worth mentioning that the method proposed here, conversely to the empirical expressions and simplified formulas commonly employed (Clough & Schmidt, 1981; Mitchell, 1983; Attewell *et al.*, 1986; Macklin, 1999), explicitly takes three key factors into consideration: (*a*) the tunnel geometry (in terms of diameter and depth); (*b*) mechanical and hydraulic soil properties; and (*c*) TBM excavation parameters (excavation rate and face pressure).

APPLICATION TO A CASE STUDY

The ground surface profile and the water table level relative to the case study are sketched in Fig. 8(a). An enlargement of the area of interest for this paper is depicted in Fig. 8(b). The stratigraphy is characterised by four geological formations; however, the laboratory test results obtained in the for-construction design stage highlighted that, from a mechanical point of view, the behaviour of the three deeper layers is coincident and therefore the tunnel is assumed to be excavated in a unique, homogeneous, normally consolidated clayey soil layer (Table 2).

The tunnel was excavated by means of an earth pressure balance TBM. The TBM head diameter was 15·08 m and the average overcut (δ) was 0·045 m. The length of the shield was 12·8 m. The segmental lining was characterised by a thickness of 60 cm and the ring was 2 m long. The backfilling was realised by using a two-component grout (water/bentonite mass ratio 20/1, cement/bentonite mass ratio 8/1) injected at a pressure 50 kPa larger than the face pressure. The spoil was extracted by means of a belt conveyor, allowing direct measurement of the spoil weight (soil + conditioning).

During the excavation process, the vertical displacements of the ground surface were monitored at cross-section A–A′ (of Fig. 8(b)). Measured settlements at the ground level are illustrated in Fig. 9. Specifically, the maximum measured displacement is related to the distance from the tunnel face in Fig. 9(a), whereas in Fig. 9(b) it is related to time. In Fig. 9(c) the final spatial settlement distribution is plotted (circle symbols).

Furthermore, owing to the presence of a parallel tunnel, a horizontal inclinometer was installed at point B (Fig. 8(b)), perpendicularly to the excavated tunnel axis (Figs 10(a) and 10(b)). This set-up allowed the designers to measure the progressive evolution of horizontal displacements caused by the tunnel face approaching. The measured values corresponding to different values of face distance are plotted in Fig. 10(c), whereas the evolution of the average values in the excavated tunnel cross-section (circles) are shown in Fig. 10(d).

In the considered area of interest (Fig. 8(b)) both ground surface and water table level are almost horizontal. The tunnel cover is equal to 112 m ($H/D \cong 7{\cdot}5$) and the water table level is located at a depth of 20 m from the ground surface.

To apply the simplified approach described in sections titled 'Meta-model for the assessment of HM coupled face extrusion' and 'Application to the case of mechanised tunnelling', the following assumptions were introduced.

(*a*) The soil mechanical/hydraulic properties and the at-rest lateral earth pressure coefficient (k_0 = 1) were derived from the for-construction design (values of Table 2 relative to limey marls).
(*b*) The values of TBM advancement rate (v_{ex} = 13·5 m/day) and face pressure ($\sigma_{f,TBM}$ = 360 kPa) are the average values measured during the excavation.
(*c*) The limit value of the average horizontal displacement in the cross-section (Fig. 10(d)) for a zero distance from the face is identified as the face extrusion.

For this reason, all the results of the simplified approach have to be interpreted as a 'blind prediction', since none of the input data was back-analysed.

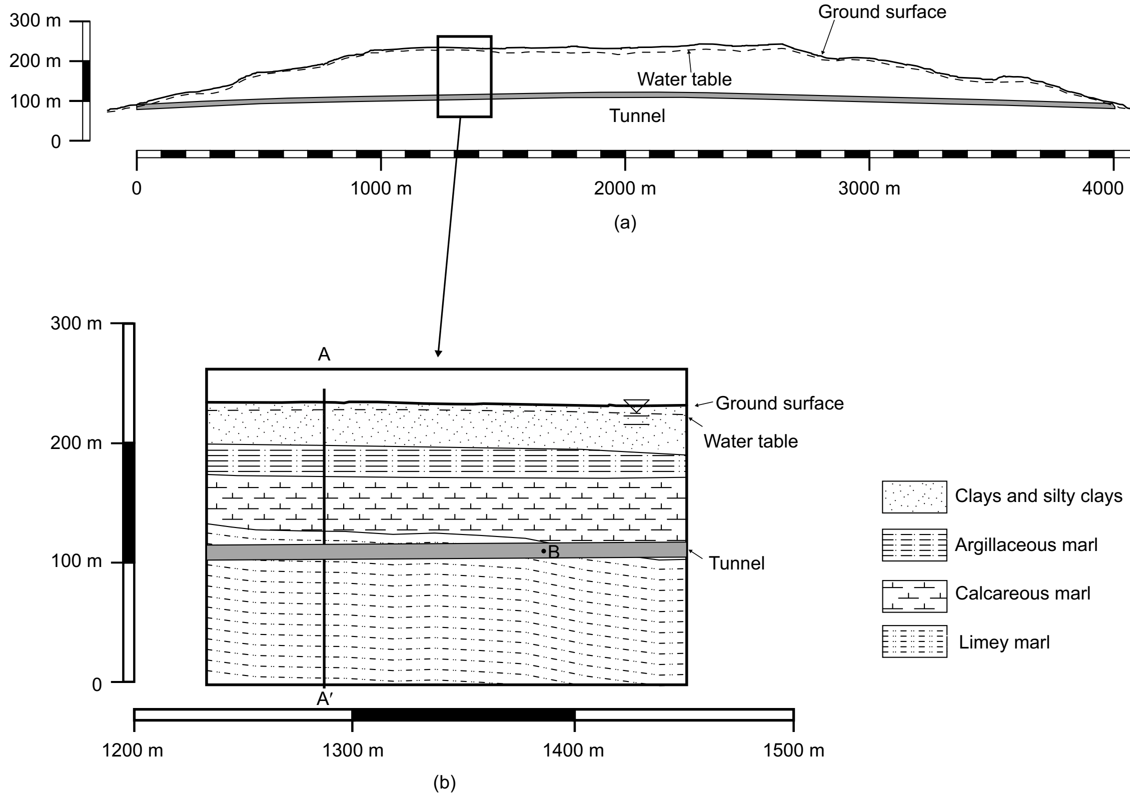

Fig. 8. (a) Sketch of the ground surface and (b) detail of the geological formations in the area of interest

Table 2. Soil mechanical/hydraulic properties (derived from for-construction design)

	Unit weight: kN/m^3	Young's modulus: MPa	Poisson's ratio	Cohesion: kPa	Friction angle: deg	Dilatancy angle: deg	Permeability: m/s
Clays and silty clays	22·3	85	0·3	5	23	0	10^{-9}
Argillaceous marls	22·3	85	0·3	0	25	0	10^{-9}
Calcareous marls	22·3	85	0·3	0	25	0	10^{-9}
Limey marls	22·3	85	0·3	0	25	0	10^{-9}

As was previously mentioned, the practical use of the approach introduced by the authors requires the definition of input data such as geometry, soil mechanical/hydraulic properties and TBM excavation parameters, and the use of the equations reported in the sections 'Meta-model for the assessment of HM coupled face extrusion' and 'Application to the case of mechanised tunnelling', as well as in Appendix 5. For the sake of clarity, a flow chart illustrating the practical employment of the approach is reported in Fig. 11. The predicted face extrusion value of 21 cm (cross symbol in Fig. 10(d)) is in very good agreement with the average values of displacements measured by the inclinometer.

The average weight of the extracted soil (excluding the conditioning weight) for each ring length (2 m), measured along the tunnel excavation, was equal to 9120 kN. By introducing the calculated value of face extrusion (21 cm) into equation (6), $W_s = 8950$ kN. Again, the agreement is very satisfactory (the error in the prediction is lower than 4%).

The surface settlement profile at the ground surface (S) is calculated by following the standard approach proposed in Peck (1969), according to which:

$$S = \frac{0{\cdot}31 V_L}{i} D^2 \exp\left(-\frac{x^2}{2i^2}\right) \tag{8}$$

where V_L is volume loss; x is the horizontal coordinate perpendicular to the tunnel axis and starting from the tunnel centre; and

$$i = k^* \left(H + \frac{D}{2}\right) \tag{9}$$

where k^* is an empirical coefficient depending on the type of soil (Mair & Taylor, 1997; di Prisco *et al.*, 2022b).

As was previously mentioned, V_L is assumed to be given by the sum of four volume loss contributions: volume loss at the tunnel face; volume loss along the shield ($V_{L,s}$); volume loss at the tail ($V_{L,t}$); and long-term volume loss due to consolidation ($V_{L,l}$).

The volume loss at the face ($V_{L,f} = 0{\cdot}9\%$) is assessed by using equation (7) in which the calculated value of face extrusion (21 cm) was introduced.

Since the face pressure is significantly lower than geostatic vertical stresses, the soil is assumed to be moving toward the cavity associated with the TBM conicity (Vu *et al.*, 2016). By following the approach proposed in Dimmock & Mair (2007):

$$V_{L,s} = \frac{4\delta}{D} = 1{\cdot}2\% \tag{10}$$

By following what was suggested in Vu *et al.* (2016), the volume loss at the tail can be calculated by using the cavity

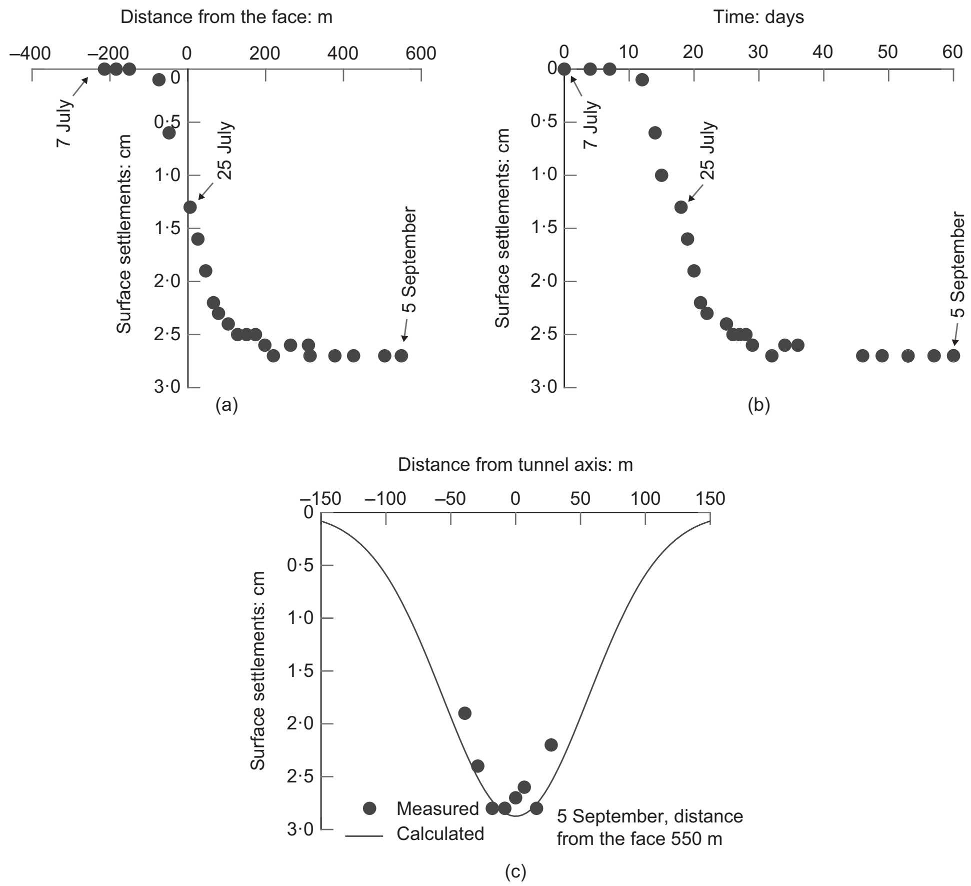

Fig. 9. Surface settlement measures in section A of Fig. 8(b): (a) evolution with distance of the face along the tunnel axis; (b) evolution with time along the tunnel axis; and (c) final values perpendicular to the tunnel axis

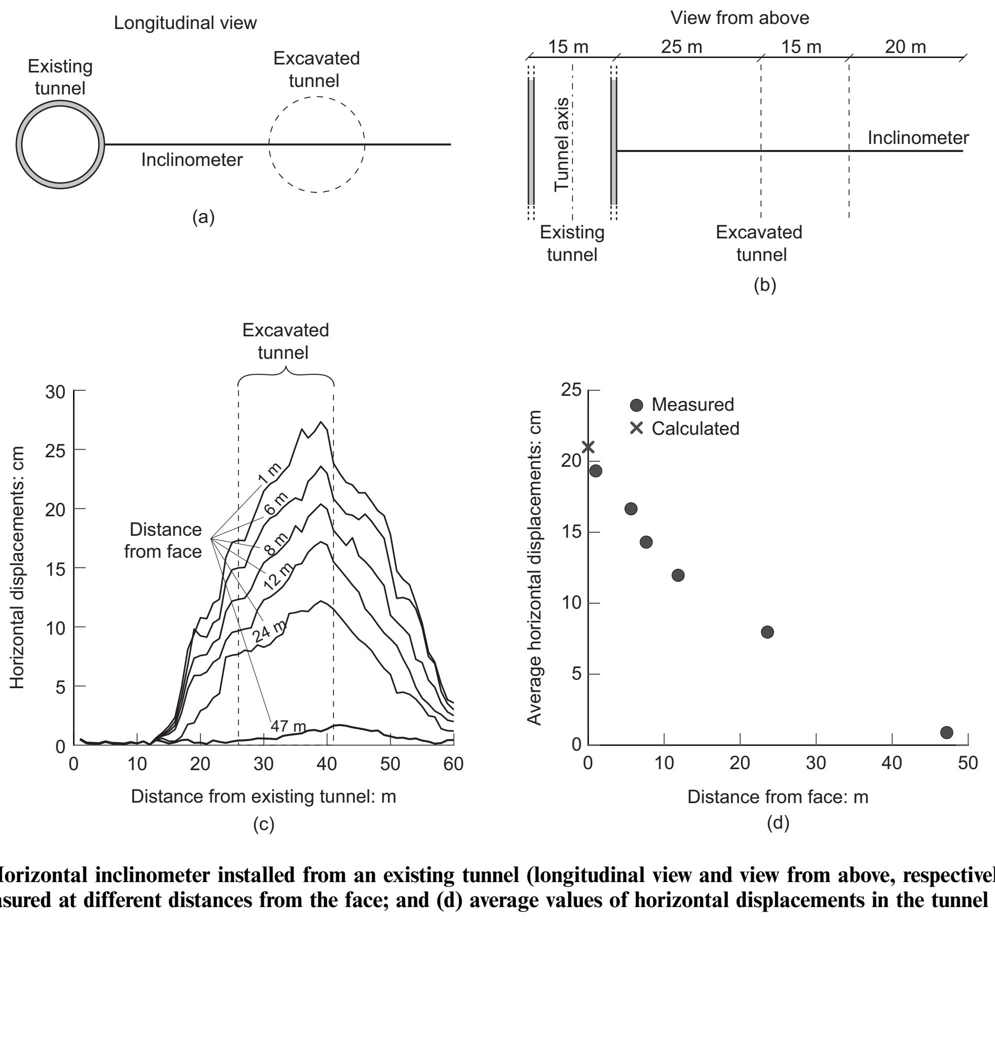

Fig. 10. (a), (b) Horizontal inclinometer installed from an existing tunnel (longitudinal view and view from above, respectively); (c) horizontal displacements measured at different distances from the face; and (d) average values of horizontal displacements in the tunnel cross-section

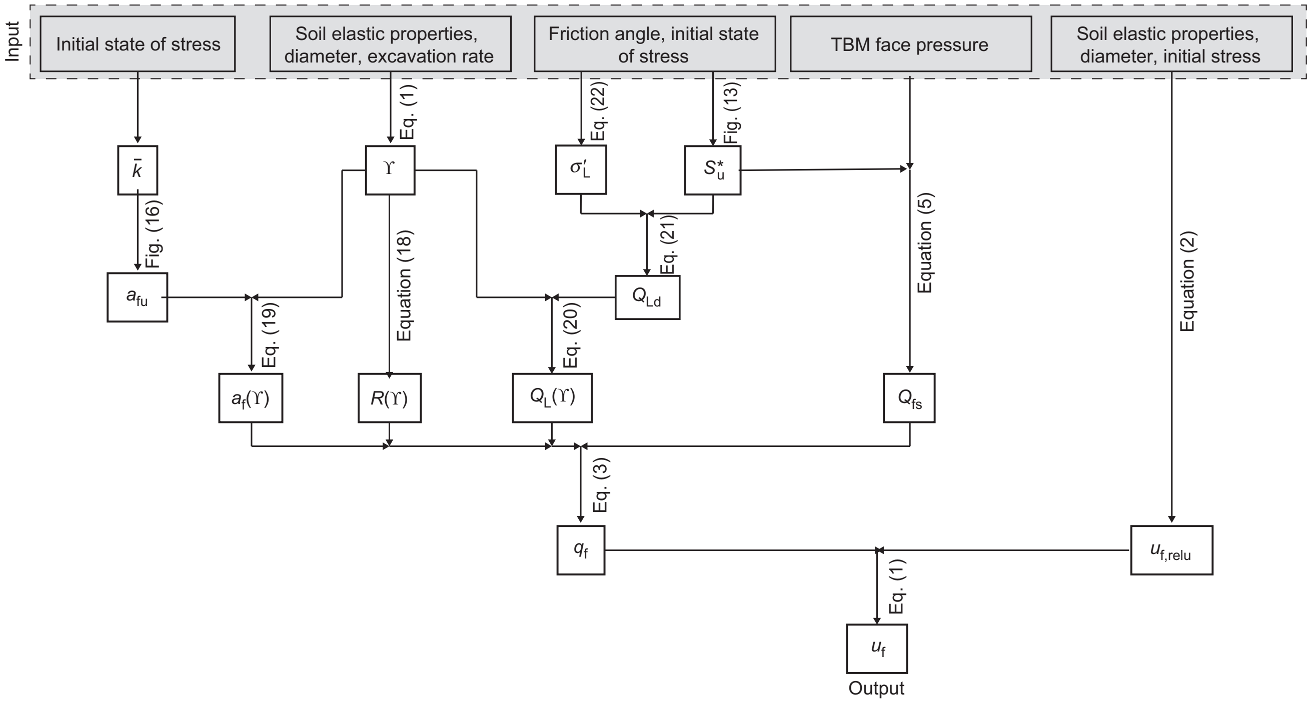

Fig. 11. Flowchart of the simplified design approach for calculating face extrusion

expansion theory. The maximum value of settlement calculated by using this theory and by using the average value of back-filling injection pressure (360 + 50 kPa) is equal to 0·8 mm. Since this value is practically negligible with respect to the measured maximum displacement values (approximately equal to 3 cm, as is shown in Fig. 9(c)), the authors assumed $V_{L,t} = 0$.

The evolution of ground surface settlements with time (Fig. 9(b)) is characterised by an almost constant trend for large time values, highlighting (in the period considered by the monitoring system) a negligible role of the consolidation process on settlements. For this reason, the authors assume $V_{L,l} = 0$.

The Gaussian curve reproducing the ground surface settlements obtained by assuming $V_L = V_{L,f} + V_{L,s} = 2{\cdot}1\%$ and $k^* = 0{\cdot}47$ is plotted in Fig. 9(c) (solid line). k^* was fitted on the experimental measures to capture the amplitude of the settlement trough. The value of k^* is in agreement with the values suggested in Mair & Taylor (1997) for clayey materials (ranging in between 0·4 and 0·6). As is evident in Fig. 9(c), the calculated settlement profile is almost coincident with the measured one (the maximum absolute error is approximately equal to 2 mm).

In the literature simplified methods, estimating volume loss dependence on excavation rate in saturated clayey soils, are not available. According to Macklin (1999), in the case given here above, $V_L = 0{\cdot}88\%$ and, by means of equation (8), the maximum settlement would be 1·1 cm, a value significantly smaller than the one measured (Fig. 9).

CONCLUDING REMARKS

In this paper an approach developed to estimate face extrusion in conventional tunnelling is extended to the case of mechanised tunnelling. The proposed approach is applicable to deep tunnels excavated in saturated clayey materials and is based on a meta-model accounting for HM coupling. By employing the novel method introduced in this paper, the calculated values of face extrusion are used to estimate spoil weight and volume loss at the tunnel face.

The model predictions were compared to measurements from a case study, and the agreement was highly satisfactory. From a practical perspective, the approach introduced by the authors can be employed during the early stages of the design process for the following purposes: (*a*) identifying the required characteristics of the TBM, such as maximum face pressure and excavation rate, when admissible surface settlements are defined; (*b*) providing preliminary cost estimates for construction.

Furthermore, during the construction phase, this method is useful in (*a*) critically interpreting monitoring data and (*b*) pre-designing suitable mitigation measures (e.g. variation in face pressure or in the excavation rate), if necessary, in cases of unforeseen or unavoidable variations in the soil profile.

The meta-model equations are implemented in a code available in GitHub (2024).

APPENDIX 1

The meta-model was conceived by interpreting the numerical results obtained by performing a series of 3D HM coupled FE numerical analyses, considering a circular tunnel of diameter *D* excavated in a homogeneous clayey soil layer (Fig. 12(a)). The tunnel cover diameter ratio (*H*/*D*) is assumed to be sufficiently large (greater than or equal to 4) to neglect the effects of the ground surface (‘deep tunnel’). The saturated soil unit weight is assumed to be constant along the depth and permeability is assumed to be isotropic and constant along the depth. The lining is assumed to be rigid.

The soil mechanical behaviour is assumed to be elastic–perfectly plastic. The elastic properties, Young’s modulus and Poisson’s ratio are assumed to be constant along the depth. The yield surface is defined by the Mohr–Coulomb criterion and the flow rule is non-associated. Despite its simplicity, this constitutive relationship can capture the main aspects of the mechanical processes taking place in the soil domain. The use of more sophisticated constitutive laws (such as strain-hardening elastic–plastic constitutive relationships) confirms this statement (Flessati & di Prisco, 2018).

On the lower and lateral boundaries of the domain, normal displacements are imposed to be zero. The water table level is assumed to be coincident with the ground surface and all the other boundaries are assumed to be impervious to water.

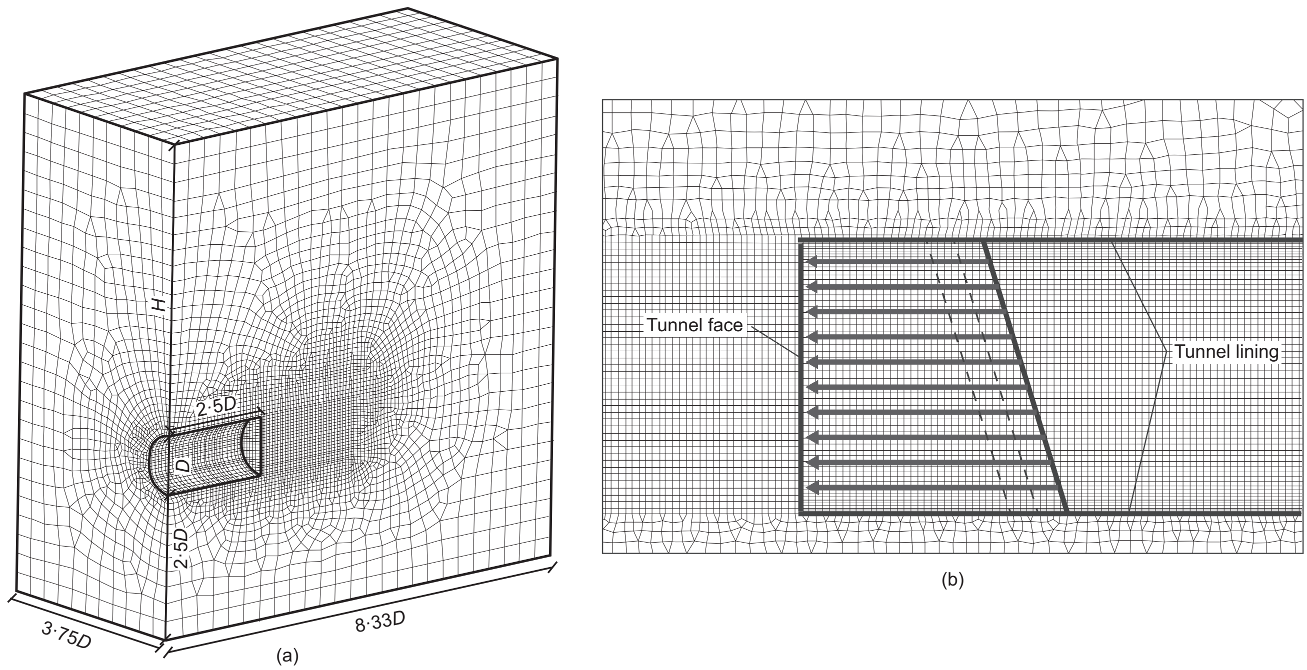

Fig. 12. (a) Numerical model and (b) progressive reduction in pressure applied at the face (adapted from di Prisco *et al.* (2018b))

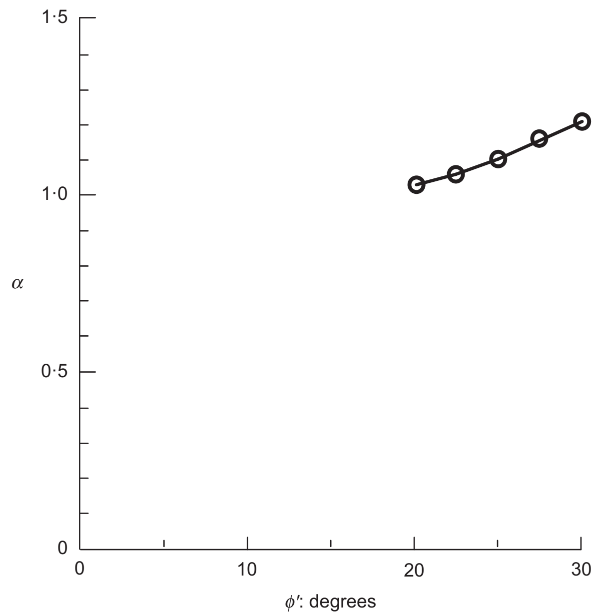

Fig. 13. Variation of α with ϕ'

In analogy to what was done in Chambon & Corté (1994), Vermeer *et al.* (2002), Sterpi & Cividini (2004), Kirsch (2009), di Prisco *et al.* (2018a, 2018b) and di Prisco *et al.* (2020), the excavation process is modelled as a progressive reduction in the pressure applied at the face (Fig. 12(b)).

APPENDIX 2

The FE numerical results (di Prisco *et al.*, 2019b) employed to introduce the meta-model were obtained by implementing a Mohr–Coulomb failure criterion and by performing HM coupled numerical analyses. This implies that, when rapid excavation processes are simulated (undrained conditions), different undrained strength (S_u) values are locally obtained according to the stress paths followed by each point belonging to the spatial domain.

As was previously mentioned, $S_u^* = \alpha S_{u,e}$ and the authors observed that α is only a function of ϕ', (Fig. 13). Fig. 13 allows calculation of α and therefore S_u^* once both the internal friction angle and tunnel axis depth are assigned.

APPENDIX 3

The influence of the excavation rate on the system response is related to excess pore water pressure dissipation. This is governed by the water mass balance equation:

$$k\left(\frac{\partial^2 h}{\partial x_1^2}+\frac{\partial^2 h}{\partial x_2^2}+\frac{\partial^2 h}{\partial x_3^2}\right) = -\frac{\partial\, \varepsilon_{vol}}{\partial t} \tag{11}$$

where h is the hydraulic head; ε_{vol} is the volumetric strain; and x_1, x_2 and x_3 define a coordinate system (hydraulic conductivity is assumed to be constant and the material is assumed to be hydraulically isotropic).

In the case where the material behaviour is assumed to obey an isotropic elastic–plastic constitutive relationship with no dilatancy:

$$\varepsilon_{vol} = \frac{p'}{K} = \frac{p - u^e - u^s}{K} \tag{12}$$

where p' and p are the effective and total pressure; u^e is the excess pore water pressure; u^s is the steady-state pore water pressure; and the soil elastic bulk modulus K is defined as follows:

$$K = \frac{E}{3(1-2v)} \tag{13}$$

By introducing u^e and u^s in the definition of the hydraulic head and by substituting ε_{vol} (equation (12)), equation (11) can be rewritten as

$$\frac{kK}{\gamma_w}\left(\frac{\partial^2 u^e}{\partial x_1^2}+\frac{\partial^2 u^e}{\partial x_2^2}+\frac{\partial^2 u^e}{\partial x_3^2}\right) = -\frac{\partial\, p}{\partial t}+\frac{\partial\, u^e}{\partial t} \tag{14}$$

By taking inspiration from the well-known one-dimensional consolidation theory, the following non-dimensional variables have been introduced:

(*a*) non-dimensional coordinates: $X_i = \dfrac{x_i}{D}$
(*b*) non-dimensional time: $T = \dfrac{t}{t_u}$
(*c*) non-dimensional excess pore water pressure: $U = \dfrac{u^e}{\sigma_{f0}}$
(*d*) non-dimensional total pressure: $P = \dfrac{p}{\sigma_{f0}}$

By introducing in equation (14) all these non-dimensional variables it reads:

$$\left(\frac{\partial^2 U}{\partial X_1^2}+\frac{\partial^2 U}{\partial X_2^2}+\frac{\partial^2 U}{\partial X_3^2}\right)=-\Upsilon\left(\frac{\partial P}{\partial T}-\frac{\partial U}{\partial T}\right) \tag{15}$$

Table 3. List of parameters varied to obtain numerical results of Fig. 14 for $H/D = 5$, $\gamma_{sat} = 20$ kN/m^3, $\nu = 0{\cdot}3$, $\phi' = 25°$, $\psi = 0°$ and $k_0 = 1 - \sin\phi'$

	D: m	E: MPa	t_u: days	k: m/s
A	12	100	1	10^{-8}
B	12	100	10	10^{-9}
C	12	1000	1	10^{-9}
D	12	1000	0·1	10^{-8}
E	0·12	100	0·0001	10^{-8}

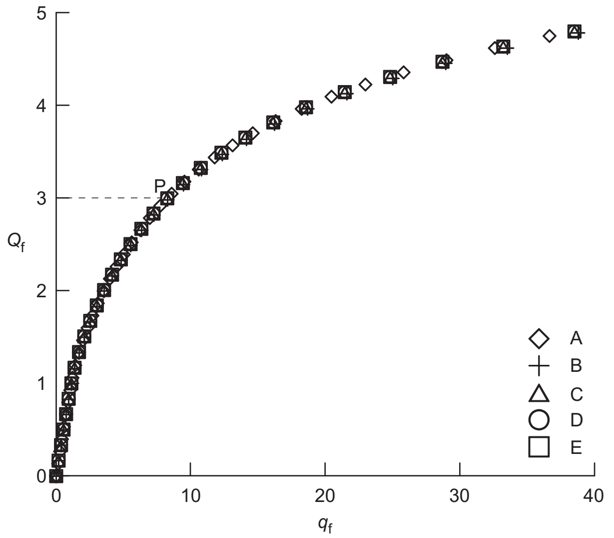

Fig. 14. Numerical results relative to $\Upsilon = 20$ (Table 3)

in which the non-dimensional excavation rate (Υ) is defined:

$$\Upsilon=\frac{\gamma_w D^2}{kKt_u}=\frac{3(1-2\nu)\gamma_w D^2}{kEt_u} \tag{16}$$

Equation (15) only depends on Υ. For this reason, once Υ is fixed, the response of the system is unique (Appendix 4) at the local level (stresses and strain distributions) and at the global one (face characteristic curve, equation (3)).

APPENDIX 4

To demonstrate that, under partially drained conditions, once Υ is defined, the response in the Q_f–q_f plane is unique, the authors performed a series of analyses characterised by $\Upsilon = 20$ and different D, k, E and t_u values (Table 3 and Fig. 14). Boundary conditions and analyses phases are those employed for the analyses discussed in the section 'Meta-model for the assessment of HM coupled face extrusion'. The perfect coincidence of these curves is due to the value of the dilatancy employed ($\psi = 0°$), which excludes any HM coupling associated with plastic strains. This also justifies the choice of employing, even if the soil behaviour is assumed to be elastic–perfectly plastic, the elastic properties in the definition of the non-dimensional excavation rate Υ (equation (1)).

The local system response is analysed in terms of non-dimensional hydraulic head (h^*), defined as

$$h^*=\frac{h-h_0}{h_0} \tag{17}$$

where h is the current hydraulic head and h_0 is the initial value of h. For the sake of brevity, only the results corresponding $Q_f = 3$ (point P of Fig. 14) for analyses A and E (Table 3) are plotted in Fig. 15 (for the sake of clarity, only a portion of the domain close to the tunnel face is represented). The hydraulic head distributions in Figs 15(a) and 15(b) are practically coincident, suggesting that the local system response is unique for fixed Υ and Q_f values.

The negative values of h^* close to the face and the positive values of h^* close to the lining clearly show that, during the face unloading process, the water will flow toward the advance core. Moreover, the increase in pore pressure close to the lining, due to the stress migration from the advance core to the lining, confirms the stress redistribution taking place in the soil domain (also experimentally observed by Nomoto *et al.* (1999) and Berthoz *et al.* (2012a)).

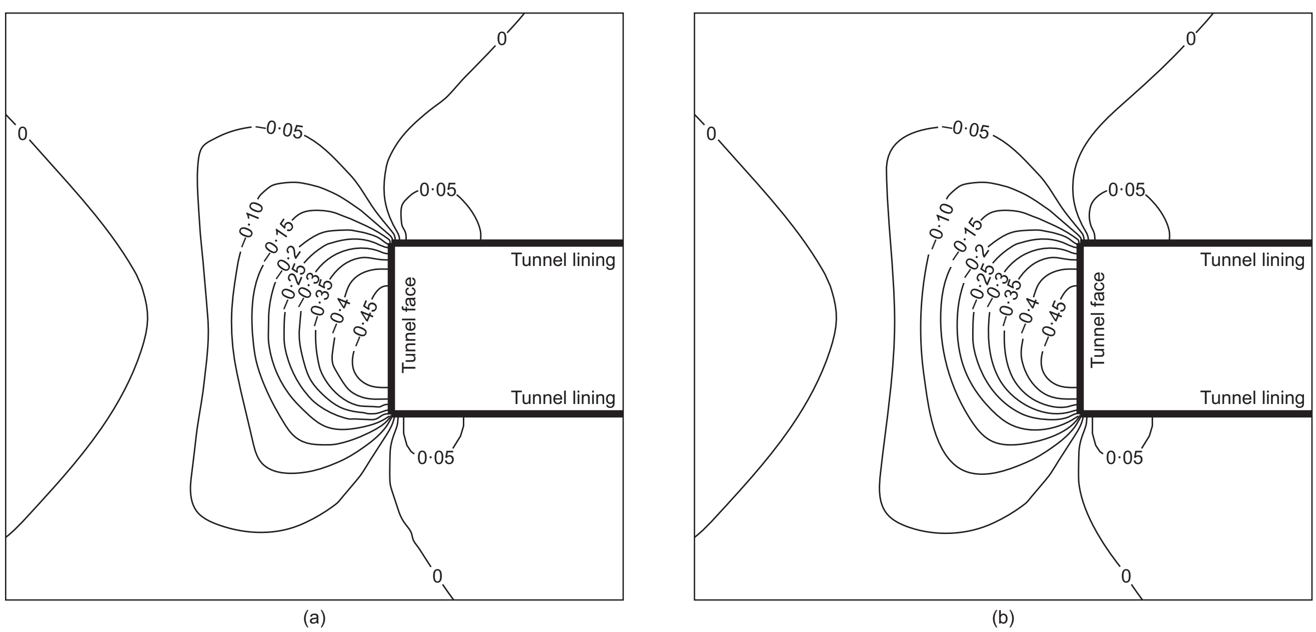

Fig. 15. Profiles of non-dimensional hydraulic head in the proximity of the face: (a) analysis A of Table 3 ($D = 12$ m); (b) analysis E of Table 3 ($D = 0{\cdot}12$ m)

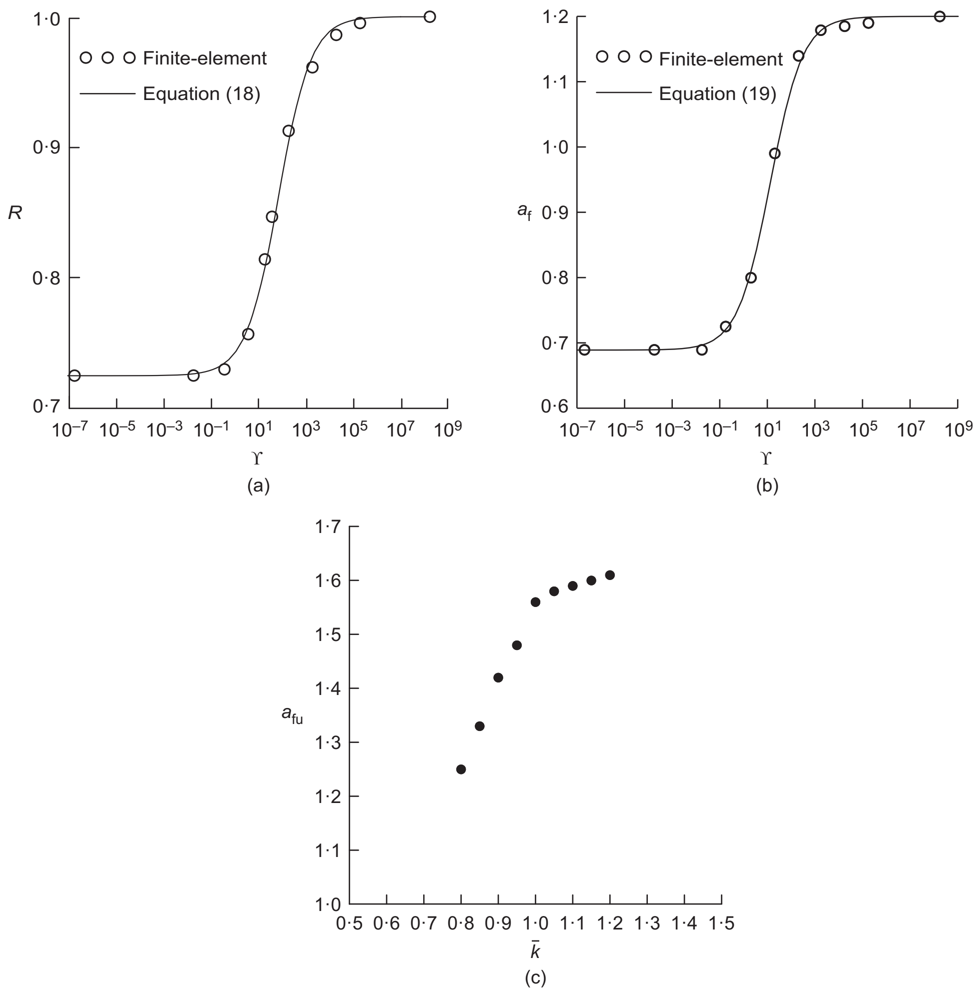

Fig. 16. (a) Variation of *R* with ϒ; (b) variation of a_f with ϒ; (c) variation of a_{fu} with $\bar{k}$, adapted from di Prisco *et al.* (2018b)

APPENDIX 5

The expressions of functions $R(\Upsilon)$, $a_f(\Upsilon)$ and $Q_L(\Upsilon)$ of equation (3) were derived from the interpolation of numerical results (di Prisco *et al.*, 2019b). In particular:

$$R(\Upsilon) = R_d + (R_u - R_d)\frac{0{\cdot}065\Upsilon^{0{\cdot}635}}{0{\cdot}065\Upsilon^{0{\cdot}635}+1} \tag{18}$$

with $R_u = 1$ being the non-dimensional undrained elastic stiffness, whereas $R_d = 0{\cdot}725$ is the corresponding drained stiffness. The numerical fitting is reported in Fig. 16(a).

$$a_f(\Upsilon) = a_{fd} + (a_{fu} - a_{fd})\frac{0{\cdot}2\Upsilon^{0{\cdot}635}}{0{\cdot}2\Upsilon^{0{\cdot}635}+1} \tag{19}$$

with $a_{fd} = 0{\cdot}686$ being the Q_f value for which yielding takes place under drained conditions, whereas a_{fu} is the corresponding undrained one. The numerical fitting is reported in Fig. 16(b). a_{fu}, as is shown in Fig. 16(c) (adapted from di Prisco *et al.* (2018b)), is not constant but a function of the initial (geostatic) total stress anisotropy factor $\bar{k}$ (i.e. the geostatic ratio of total horizontal and total vertical stresses).

$$Q_L(\Upsilon) = Q_{Ld} + 1{\cdot}6\Upsilon \tag{20}$$

where

$$Q_{Ld} = \frac{\sigma'_{f0} - \sigma'_L}{S_u^*} \tag{21}$$

is the non-dimensional limit value of Q_f under drained conditions; σ'_{f0} is the average effective horizontal geostatic stress applied on the tunnel face; whereas σ'_L is the minimum average effective pressure to be applied on the face to prevent its collapse under drained conditions, calculated according to Vermeer *et al.* (2002) as follows:

$$\sigma'_L = (\gamma_{sat} - \gamma_w)D\left(\frac{1}{9\tan\phi'} - 0{\cdot}05\right) \tag{22}$$

NOTATION

a_f	transition from linear to non-linear response in characteristic curves
a_{fd}	drained value of a_f
a_{fu}	undrained value of a_f
c'	cohesion
D	tunnel diameter
E	soil elastic Young's modulus
H	tunnel cover
h	hydraulic head
h^*	non-dimensional hydraulic head
h_0	initial hydraulic head
i	$= k^*\left(H + \frac{D}{2}\right)$
K	elastic bulk modulus
K_{el}	non-dimensional elastic parameter
k	permeability
k^*	amplitude of the Gaussian settlement curve
$\bar{k}$	geostatic total stress anisotropy
k_0	at-rest lateral earth pressure
L_a	distance from the face at which stresses are practically not affected by the excavation
L_r	lining segment length
M_e	$= 6\sin\phi'/(3 + \sin\phi')$
P	non-dimensional total pressure
p', p	effective pressure, total pressure
p^*	geostatic effective pressure at tunnel axis depth

Q_f, q_f non-dimensional stress on the face and non-dimensional face extrusion
Q_fs, q_fs supported Q_f and q_f
Q_fus, q_fus unsupported Q_f and q_f
Q_L limit value of Q_f
Q_Ld drained limit value of Q_f
q_adm non-dimensional admissible displacement
R inclination of non-dimensional characteristic curves
S settlements
S_u^* soil strength parameter
$S_\mathrm{u,e}$ undrained strength under extension stress paths
t time
t_u time to excavate L_a
U non-dimensional excess pore water pressure
u^e excess pore water pressure
u_f average face displacements
$u_\mathrm{f,adm}$ admissible face extrusion
$u_\mathrm{f,relu}$ undrained elastic residual (i.e. for $\sigma_\mathrm{f} = 0$) face extrusion
u^s steady-state pore water pressure
V_L volume loss
$V_\mathrm{L,f}$ volume loss at the face
$V_\mathrm{L,l}$ volume loss for long-term effects
$V_\mathrm{L,s}$ volume loss at the shield
$V_\mathrm{L,t}$ volume loss at the tail
v_ex excavation rate
W_e volume of spoil associated with excavation rate
W_r ideal spoil volume
W_s spoil volume
$x_1, x_2, x_3, X_1, X_2, X_3$ dimensional and non-dimensional coordinates
α strength parameter
γ_sat soil saturated unit weight
γ_w water unit weight
δ average overcut
ε_vol volumetric strains
ν Poisson's ratio
σ_f average stress on the face
σ_f0 geostatic average stress on the face
$\sigma_\mathrm{f,TBM}$ pressure applied on the tunnel face by the TBM head
σ'_L limit effective pressure on the face
Υ non-dimensional excavation rate
ϕ' soil internal friction angle
ψ dilatancy

REFERENCES

Anagnostou, G. & Kovari, K. (1996). Face stability conditions with earth-pressure-balanced shields. *Tunn. Undergr. Space Technol.* **11**, No. 2, 165–173.

Attewell, P. & Farmer, I. (1974). Ground disturbance caused by shield tunnelling in a stiff, overconsolidated clay. *Engng Geol.* **8**, No. 4, 361–381.

Attewell, P. B., Yeates, J. & Selby, A. R. (1986). *Soil movements induced by tunnelling and their effects on pipelines and structures.* Glasgow, UK: Blackie.

Berthoz, N., Branque, D., Wong, H., Généreux, G., Subrin, D. & Humbert, E. (2012a). Tunneling in stratified soft ground: experimental study on 1*g* EPBS reduced scale model. In *Geotechnical aspects of underground construction in soft ground – proceedings of the 7th international symposium on geotechnical aspects of underground construction in soft ground* (ed. G. Viggiani), pp. 411–416. Leiden, The Netherlands: CRC Press/Balkema.

Berthoz, N., Branque, D., Subrin, D., Wong, H. & Humbert, E. (2012b). Face failure in homogeneous and stratified soft ground: theoretical and experimental approaches on 1g EPBS reduced scale model. *Tunn. Undergr. Space Technol.* **30**, 25–37.

Callari, C. (2004). Coupled numerical analysis of strain localization induced by shallow tunnels in saturated soils. *Comput. Geotech.* **31**, No. 3, 193–207.

Callari, C. (2015). Numerical assessment of tunnel face stability below the water table. *Proceedings of the 14th IACMAG*, Kyoto, Japan, pp. 2007–2010. London, UK: Taylor & Francis Group.

Callari, C. & Casini, S. (2006). Three-dimensional analysis of shallow tunnels in saturated soft ground. In *Geotechnical aspects of underground construction in soft ground – proceedings of the 5th international conference of TC28 of the ISSMG* (eds K. J. Bakker, A. Bequijen, W. Broere and E. A. Kwast), pp. 495–502. Leiden, The Netherlands: Taylor & Francis/Balkema.

Callari, C., Alsahly, A. & Meschke, G. (2017). Assessment of stand-up time and advancement rate effects for tunnel faces below the water table. In *4th ECCOMAS conference on computational methods in tunneling and subsurface engineering (EURO:TUN 2017),* Innsbruck, Austria (eds G. Hofstetter, K. Bergmeister, J. Eberhardsteiner, G. Meschke and H. F. Schweiger).

Chambon, P. & Corté, J. F. (1994). Shallow tunnels in cohesionless soil: stability of tunnel face. *J. Geotech. Engng* **120**, No. 7, 1148–1165.

Chen, R. P., Li, J., Kong, L. G. & Tang, L. J. (2013). Experimental study on face instability of shield tunnel in sand. *Tunn. Undergr. Space Technol.* **33**, 12–21.

Clough, G. & Schmidt, B. (1981). The design and performance of excavations and tunnels. In *Soft clay engineering, developments in geotechnical engineering* (eds E. W. Brand and R. P. Brenner), Ch. 8, pp. 567–634. Elsevier Scientific Publishing Company.

Cording, E. & Hansmire, W. (1975). Displacements around soft ground tunnels. *5th Pan American congress on soil mechanics and foundation engineering*, Buenos Aires, pp. 571–632. Paris, France: Sovim.

Davis, E. H., Gunn, M. J., Mair, R. J. & Seneviratine, H. N. (1980). The stability of shallow tunnels and underground openings in cohesive material. *Géotechnique* **30**, No. 4, 397–416, https://doi.org/10.1680/geot.1980.30.4.397.

Dimmock, P. S. & Mair, R. J. (2007). Estimating volume loss for open-face tunnels in London Clay. *Proc. Instn Civ. Engrs – Geotech. Engng* **160**, No. 1, 13–22, https://doi.org/10.1680/geng.2007.160.1.13.

di Prisco, C., Flessati, L., Frigerio, G., Castellanza, R., Caruso, M., Galli, A. & Lunardi, P. (2018a). Experimental investigation of the time-dependent response of unreinforced and reinforced tunnel faces in cohesive soils. *Acta Geotech.* **13**, No. 3, 651–670.

di Prisco, C., Flessati, L., Frigerio, G. & Lunardi, P. (2018b). A numerical exercise for the definition under undrained conditions of the deep tunnel front characteristic curve. *Acta Geotech.* **13**, No. 3, 635–649.

di Prisco, C., Flessati, L., Cassani, G. & Perlo, R. (2019a). Influence of the fibreglass reinforcement stiffness on the mechanical response of deep tunnel fronts in cohesive soils under undrained conditions. In *Tunnels and underground cities: engineering and innovation meet archaeology, architecture and art* (eds D. Peila, G. Viggiani and T. Celestino), pp. 1323–1331. Leiden, The Netherlands: CRC Press/Balkema.

di Prisco, C., Flessati, L., Cassani, G. & Perlo, R. (2019b). Influence of the excavation rate on the mechanical response of deep tunnel fronts in cohesive soils. In *Tunnels and underground cities: engineering and innovation meet archaeology, architecture and art* (eds D. Peila, G. Viggiani and T. Celestino), pp. 3654–3663. Leiden, The Netherlands: CRC Press/Balkema.

di Prisco, C., Flessati, L. & Porta, D. (2020). Deep tunnel fronts in cohesive soils under undrained conditions: a displacement-based approach for the design of fibreglass reinforcements. *Acta Geotech.* **15**, No. 4, 1013–1030, https://doi.org/10.1007/s11440-019-00840-8.

di Prisco, C., Boldini, D., Desideri, A., Bilotta, E., Russo, G., Callari, C., Flessati, L., Graziani, A. & Meda, A. (2022a). Computational methods. In *Handbook on tunnels and underground works* (eds E. Bilotta, R. Casala, C. Giulio di Prisco, S. Miliziano, D. Peila, A. Pigorini and E. M. Pizzarotti), pp. 203–245. Leiden, The Netherlands: CRC Press/Balkema.

di Prisco, C., Callari, C., Barbero, M., Bilotta, E., Russo, G., Boldini, D., … & Sciotti, A. (2022b). Assessment of excavation-related hazards and design of mitigation measures. In *Handbook on tunnels and underground works* (eds E. Bilotta,

R. Casala, C. Giulio di Prisco, S. Miliziano, D. Peila, A. Pigorini and E. M. Pizzarotti), pp. 247–316. Leiden, The Netherlands: CRC Press/Balkema.

Flessati, L. (2017). *Mechanical response of deep tunnel fronts in cohesive soils: experimental and numerical analyses.* PhD thesis, Politecnico di Milano, Milan, Italy.

Flessati, L. & di Prisco, C. (2018). Numerical investigation on the influence of the excavation rate on the mechanical response of deep tunnel fronts in cohesive soils. In *Proceedings of China-Europe conference on geotechnical engineering*, Vienna, Austria (eds W. Wu and H.-S. Yu), Springer Series in Geomechanics and Geoengineering, pp. 1140–1143. Cham, Switzerland: Springer.

Flessati, L. & di Prisco, C. (2022). A displacement-based approach for a face pressure assessment in mechanized tunnelling. *EURO: TUN 2021, 5th international conference on computational methods and information models in tunneling, 22–24 June 2022*. Bochum, Germany: Ruhr University Bochum.

Flessati, L. & di Prisco, C. (2023). Deep tunnel faces in cohesive soils under undrained conditions: application of a new design approach. *Eur. J. Civ. Environ. Engng* **27**, No. 8, 2630–2644, https://doi.org/10.1080/19648189.2020.1785332.

GitHub (2024). https://github.com/LFlessati/TunnelFace (accessed 09/04/2024).

Höfle, R., Fillibeck, J. & Vogt, N. (2008). Time dependent deformations during tunnelling and stability of tunnel faces in fine-grained soils under groundwater. *Acta Geotech.* **3**, 309–316.

Höfle, R., Fillibeck, J. & Vogt, N. (2009). Time depending stability of tunnel face. In *Proceedings of 35th ITA-AITES general assembly*, Budapest, Hungary.

Horn, N. (1961). Horizontaler erddruck auf senkrechte abschlussflächen von tunnelröhren. In *Landeskonferenz der ungarischen tiefbauindustrie*, Budapest, Hungary.

Hu, X., Fang, Y., Walton, G. & He, C. (2022). Laboratory model test of slurry shield tunnelling in saturated sandy soil. *Géotechnique* **73**, No. 10, 885–906, https://doi.org/10.1680/jgeot.21.00066.

Kamata, H. & Mashimo, H. (2003). Centrifuge model test of tunnel face reinforcement by bolting. *Tunn. Undergr. Space Technol.* **18**, No. 2, 205–212.

Kimura, T. & Mair, R. (1981). Centrifugal testing of model tunnels in soft clay. In *Proceedings of the 10th international conference on soil mechanics and foundation engineering*. London, UK: International Society for Soil Mechanics and Foundation Engineering (ISSMFE).

Kirsch, A. (2009). *On the face stability of shallow tunnels in sand*. PhD thesis, Innsbruck University, Innsbruck, Austria.

Klar, A., Osman, S. & Bolton, M. (2007). 2D and 3D upper bound solutions for tunnel excavation using 'elastic' flow fields. *Int. J. Numer. Analyt. Methods Geomech.* **31**, No. 12, 1367–1374.

Kratz, B., Jehel, P. & Tatin, M. (2023). 3D numerical simulation of TBM excavation for predicting surface settlements – state of the art. In *Expanding underground – knowledge and passion to make a positive impact on the world* (eds G. Anagnostou, A. Benardos and V. P. Marinos), pp. 2757–2765. CRC Press.

Leca, E. & Dormieux, L. (1990). Upper and lower bound solutions for the face stability of shallow circular tunnels in frictional material. *Géotechnique* **40**, No. 4, 581–606, https://doi.org/10.1680/geot.1990.40.4.581.

Macklin, S. (1999). The prediction of volume loss due to tunnelling in overconsolidated clay based on heading geometry and stability number. *Ground Engng* **32**, No. 4, 30–33.

Mair, R. (1979). *Centrifugal modelling of tunnel construction in soft clay.* PhD thesis, Cambridge University, Cambridge, UK.

Mair, R. & Taylor, R. (1997). Theme lecture: bored tunnelling in the urban environment. *Proceedings of XIV ICSMFE*, 1999. London, UK: International Society for Soil Mechanics and Geotechnical Engineering.

Mitchell, R. J. (1983). *Earth structure engineering*. Winchester, MA, USA: Allen & Unwin Inc.

Mollon, G., Dias, D. & Soubra, A. H. (2009). Face stability analysis of circular tunnels driven by a pressurized shield. *J. Geotech. Geoenviron. Engng* **136**, No. 1, 215–229.

Mollon, G., Dias, D. & Soubra, A. H. (2013). Continuous velocity fields for collapse and blowout of a pressurized tunnel face in purely cohesive soil. *Int. J. Numer. Analyt. Methods Geomech.* **37**, No. 13, 2061–2083.

Mühlhaus, H. B. (1985). Lower bound solutions for circular tunnels in two and three dimensions. *Rock Mech. Rock Engng* **18**, No. 1, 37–52.

Nomoto, T., Imamura, S., Hagiwara, T., Kusakabe, O. & Fujii, N. (1999). Shield tunnel construction in centrifuge. *J. Geotech. Geoenviron. Engng* **125**, No. 4, 289–300.

Peck, R. B. (1969). Deep excavations and tunneling in soft ground. *Proceedings of 7th ICSMFE*, pp. 225–290. London, UK: International Society for Soil Mechanics and Geotechnical Engineering.

Pferdekämper, T. & Anagnostou, G. (2022). Undrained trapdoor and tunnel face stability revisited. *Géotechnique Lett.* **12**, No. 4, 1–7, https://doi.org/10.1680/jgele.22.00053.

Shang, W., Song, Z., Chen, Z., Chen, T., Meng, J. & Zheng, X. (2023). Experimental investigation of face stability of a slurry shield tunnel based on a newly developed model test system. *Geotech. Geol. Engng* **41**, No. 7, 4137–4152.

Sitarenios, P. & Kavvadas, M. (2016). The interplay of face support pressure and soil permeability on face stability in EPB tunneling. In *Proceedings of WTC16*, San Francisco, CA, USA, pp. 2514–2523. San Francisco, CA, USA: Society for Mining, Metallurgy and Exploration Englewood.

Soe, T. E. E. & Ukritchon, B. (2023). Three-dimensional undrained face stability of circular tunnels in non-homogeneous and anisotropic clays. *Comput. Geotech.* **159**, 105422.

Sterpi, D. & Cividini, A. (2004). A physical and numerical investigation on the stability of shallow tunnels in strain softening media. *Rock Mech. Rock Engng* **37**, No. 4, 277–298.

Vermeer, P. A., Ruse, N. & Marcher, T. (2002). Tunnel heading stability in drained ground. *Felsbau* **20**, No. 6, 8–18.

Vu, M. N., Broere, W. & Bosch, J. (2016). Volume loss in shallow tunnelling. *Tunn. Undergr. Space Technol.* **59**, 77–90.

Wong, H. & Subrin, D. (2006). 'Stabilité frontale d'un tunnel: mécanisme 3D en forme de corne et influence de la profondeu,'. *Rev. Eur. Génie Civ.* **10**, No. 4, 429–456 (in French).